

BUILDING DAMAGE MAPPING USING CHANGE DETECTION OF ALOS-2 PALSAR-2 SAR IMAGES AND STRONG MOTION DATA

Luis Moya¹, Erick Mas², Bruno Adriano³, Shunichi Koshimura⁴, Fumio Yamazaki⁵

¹ Researcher, IRIDeS, Tohoku University, Sendai, Japan, lmoyah@irides.tohoku.ac.jp

² Associate Professor, IRIDeS, Tohoku University, Sendai, Japan, mas@irides.tohoku.ac.jp

³ JSPS researcher fellow, IRIDeS, Tohoku University, Sendai, Japan, adriano@irides.tohoku.ac.jp

⁴ Professor, IRIDeS, Tohoku University, Sendai, Japan, koshimura@irides.tohoku.ac.jp

⁵ Professor, Chiba University, Chiba, Japan, fumio.yamazaki@faulty.chiba-u.jp

ABSTRACT: The estimation of building damage due to earthquakes is crucial for disaster management and disaster relief activities. So far, mainly two methodologies have been applied: (1) a combination of the spatial distribution of strong ground motion intensity and building damage functions; and (2) the application of change detection methodologies using satellite images such as synthetic aperture radar (SAR) data. It has been reported elsewhere that there is a correlation between changes in the backscattering coefficient and the presence of building damage. Furthermore, from a seismic hazard and risk analysis perspective, there is also a relationship between the ground motion intensity (Peak Ground Acceleration - PGA or Peak Ground Velocity - PGV) and the level of building damage, which is the foundation of fragility functions theory. However, a combination of these two methodologies to estimate building damage has not been researched much. Thus, this study aims to estimate the distribution of building damage by joining these two sources of information: change detection of pre- and post-event SAR images and spatial distribution of strong motion intensity. Building damage surveyed at Mashiki town due to the 2016 Mw7.0 Kumamoto earthquake is used as ground truth data to verify our hybrid method.

KEY WORDS: The 2016 Kumamoto earthquake, Building damage, ALOS-2 PALSAR 2

1. INTRODUCTION

Earthquake-induced building damage estimation is critical for a quick response such as sending first aid and relief. Thus, the most precise estimation the better decisions can be made during emergency disaster.

Remote sensing technology, such as optical and synthetic aperture radar (SAR) satellite images, has been used lately during several natural disasters to measure the extension of damage (Liu et al. 2013). Basic approaches rely on identifying changes between two images taken before and after a disaster event. It relies on the assumption that the changes are correlated with the effects of the earthquake.

The averaged pixel difference, correlation coefficient, and coherence between the pair of images are parameters often used to detect changes (Liu et al. 2013). Here, the main challenge is to set a threshold that separates the damage and non-damaged areas, which is challenging for low-resolution images and when large level of noise is presented.

A different approach for estimation of damage scenario is used in seismic risk analysis. Here, based on survey of previous events or numerical simulations, it is proved that an asset (i.e., buildings, bridges or structural elements) are more likely to experience damage when the engineering demand parameter (EDP), such as strong-motion intensity or tsunami inundation height, is large.

The approach uses fragility curves, which gives the probability that an element under a certain level of EDP has reached or exceeded certain level of damage (Koshimura et al. 2009).

This paper introduces a novel procedure in which a combination between change detection of a pair of SAR satellite image and spatial distribution of the EDP.

2. PRINCIPLE OF THE METHOD

A method to detect damages from satellite images consists on mapping changes of backscattering for SAR data or sun reflectance radiation for optical images. Those changes are mainly based on thresholds such as the proposed by Liu et al. (2013). During this process, uncertainties in the damage classification due to speckle noise and/or low resolution of the image are introduced. Furthermore, if the dates of the pre- or post-event image are far from the disaster date, modifications of the surface due to other reasons (i.e., new construction and harvesting activities) than the disaster might be leading to misclassification of the damaged areas.

The method proposed in this paper attempts to improve the damage classification by including the spatial distribution of EDP. This will increase the dimensionality of the problem and enrich the data set. A flowchart of the methodology is shown in Fig 1, and the steps of the algorithm are as follows:

(1) Input a pair of pre- and post-event SAR images and the spatial distribution of EDP. The SAR images here were converted from digital number to sigma naught (σ^0), which means that a preprocessing of the raw data has to be performed in advance. The EDP varies according to which natural disaster is been dealt. The strong ground motion intensity for earthquakes (PGV, PGA, etc) and the tsunami inundation depth are such examples.

(2) Calculate the parameters d and r using the pair of SAR images. For a given pixel, d and r are the difference of the average backscattering and the correlation coefficient of surrounding pixels limited by a specified window, respectively.

(3) Define the tile units. Tiles are rectangular segments considered as units, where its damage classification is desired. For each tile an average of d and r are associated. In this paper a tile is selected as the unit. However, other options such as pixel based or areas based on segmentation can be used.

(4) Extract the magnitude of the EDP for each unit.

(5) The tiles are grouped into bins by ranges of EDP, where the ranges are defined in order to have approximately the same number of tiles in each bin.

(6) Here, the main part of the method begins. The purpose here is to find an improved linear threshold with the aid of the spatial distribution of EDP.

First, an initial value of the vector parameter ($x=[x_1, x_2]$) for the threshold line: $r=x_1+x_2d$ is defined. Tiles with its pair values (d, r) below the threshold line are classified as damaged. Then, a fragility curve; i.e., a logarithmic cumulative Gaussian distribution function is fitted and the error between the damage ratio of the tiles and the fragility curve is stored. Details about the fitting process and further literature is found in Koshimura et al. (2009) and Mas et al. (2012).

(7) The next step is an iterative process to find the parameters that minimizes the fitting error between the damage ratio and the fragility curve, hereafter referred as cost function. Figure 1, shows a grid search approach. A grid search algorithm demands significant, however, other algorithms to find global minimum are possible to replace here. At this stage we aim to present the method pipeline and observe the surface of the cost function produced in the bi-dimensional space of x_1 and x_2 .

(8) Use the final threshold line to map the damage distribution.

3. EXPERIMENTAL RESULTS AND ANALYSIS

To demonstrate the performance of the method, the 2016 Mw 7.0 Kumamoto earthquake is selected as case study. The event was composed of two big earthquakes, the denominated foreshock (April 14, 2016) and the mainshock (April 16), and subsequent aftershocks. The mainshock produced extensive damage in Mashiki town and some parts of Nishihara village, Kashima and Mifune towns (Figure 2c).

Two ALOS-2 PALSAR-2 intensity images taken on March 07 2016 and April 18 2016 are used for the change detection analysis. The images were acquired in StripMap mode with HH polarization. The incident angle is 32.8 degrees and the path was descending. The backscattering coefficient (sigma naught) is obtained from the intensity images after a radiometric calibration, terrain correction and Lee filter. The parameters d and r are calculated with a window size 3x3 pixels.

The tiles are square segments of approximately 130 x 130 m² (green squares shown in Figure 2c). Tiles were selected under the criterion that each tile has at least 30 buildings inside it in order to evaluate areas with high density of buildings. The georeferenced building inventory used to define the tiles is shown as blue polygons in Figure 2b. The building inventory was obtained from the Geospatial Information Authority of Japan (GSI). A total of 1277 tiles were defined

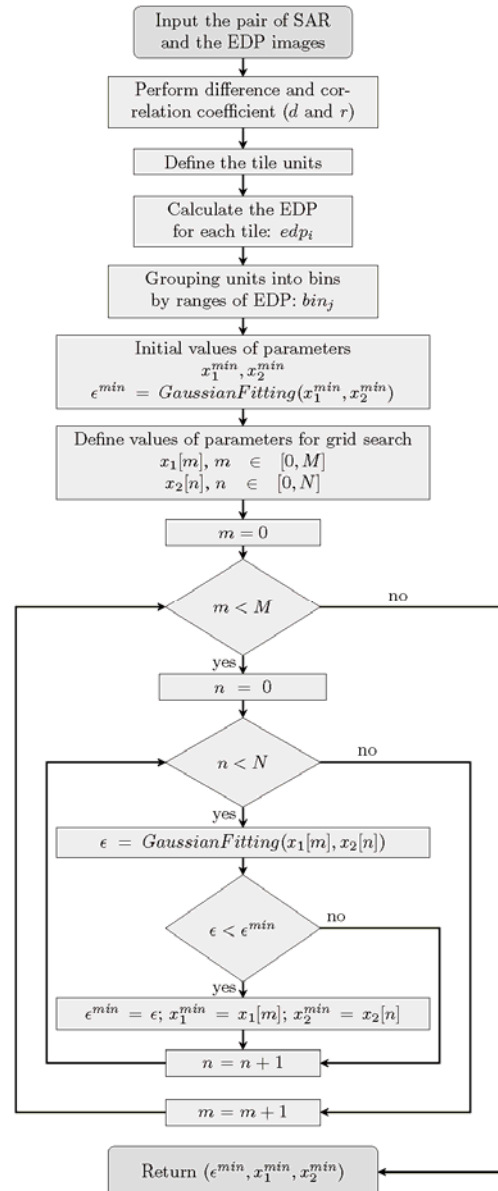


Figure 1 flowchart of the proposed method

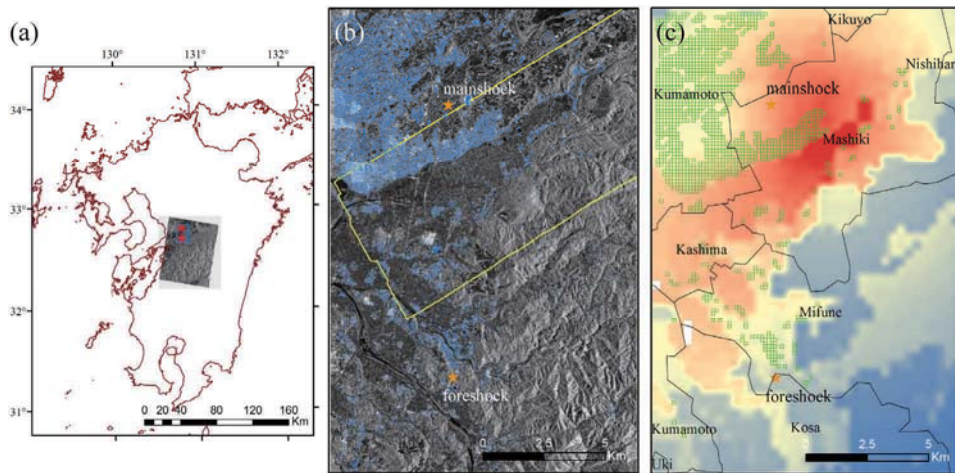


Figure 2 Location of the case study. (a) Location of the SAR images in Kyushu island, Japan and the pre-event SAR image. (b) Study area. Blue and yellow polygons represent the building foot print and the truth data, respectively. (c) Distribution of the PGV and tiles (green polygons).

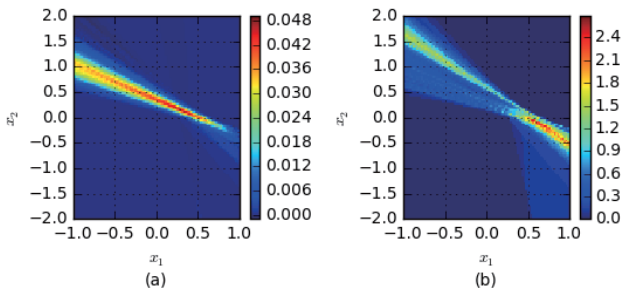


Figure 3 (a) slope of linear fitting between bins and damage ratio. (b) Cost function.

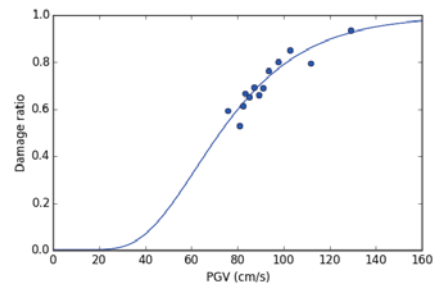


Figure 4 Best fitting of the damage ratio and a logarithmic cumulative distribution function.

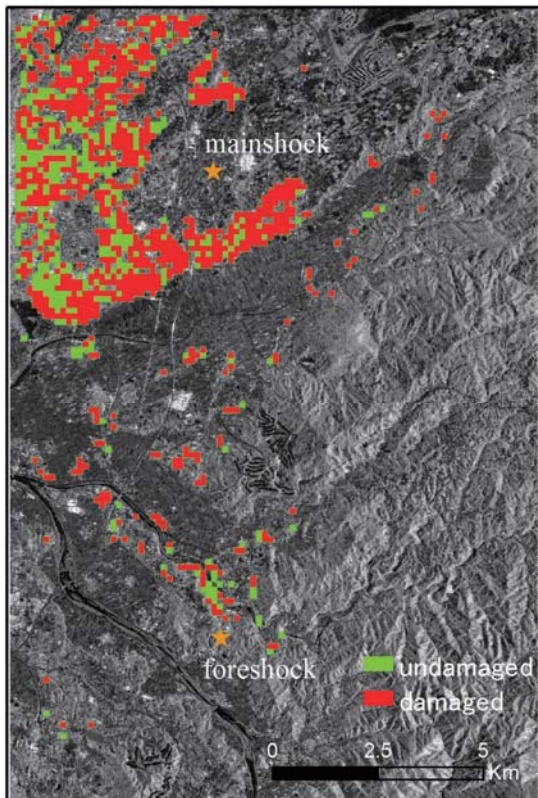


Figure 5 Spatial distribution of damaged (red tiles) and undamaged (green tiles) areas.

The spatial distribution of PGV is selected as the EDP (Figure 2c). The reason on behalf of this choice rely on the proposed empirical fragility curves for buildings in Japan (Yamazaki and Murao, 2000), where the PGV was selected as EDP. The PGV map was obtained from the QuiQuake system, a web-based system for estimation of strong ground motion maps (Matsuoka and Yamamoto 2012). The original resolution of 300 m was resampled to 10 m by cubic interpolation.

Figure 3b shows the cost function surface of the fitting process expressed as shade colors. Errors close to zero are observed in a wide area (dark blue). However, those cases occur for thresholds that produce 100% or 0% of damage ratio in all bins. Although totally collapsed or zero collapse of building is indeed theoretically possible, in practice remote sensing is used when a presence of damaged is implicit. Furthermore, the extension of a satellite image usually covers an area bigger than the affected area. Thus, we filter damage scenarios that does not shows an increment in the damage ratio when the PGV increases. Figure 3a shows the slope of a line fitted from the bin-damage ratio relation. We filtered the damage scenarios that show slope values under half of the maximum computed value in order not to consider the cases mentioned above. Although not shown here, the 50% criterion does not have big effect on the results.

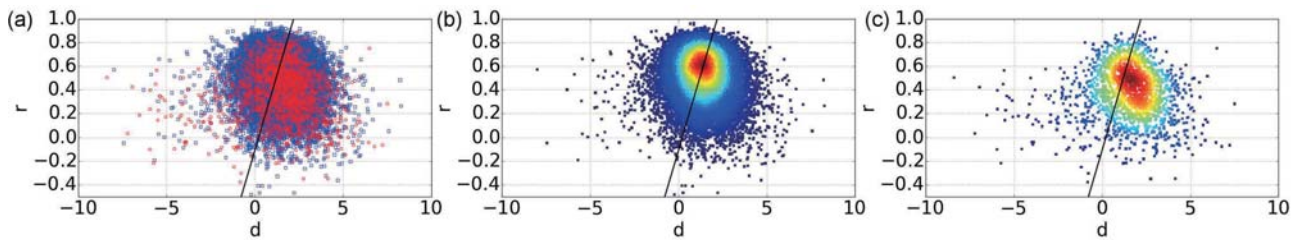


Figure 6 Scatter plot of the parameters r and d for buildings footprint and the threshold defined by the proposed method (black line). (a) undamaged buildings as blue marks and damaged building as red marks. (b) density points of undamaged buildings. (c) density points of damaged buildings.

The same results were obtained filtering results with slope less than 10% of the maximum computed value.

Figure 4 shows the final logarithmic distribution function obtained using the parameters that produced the lowest cost function among those scenarios shown before. The final threshold is expressed as follow:

$$r = -0.11 + 0.50d \quad (1)$$

It is observed that all bins shows damage ratio greater than 40%, which seems very high. Figure 5 shows the spatial distribution of the damaged area. The results show concentrated damage in Mashiki town, which shows good agreement with previous reports (Yamazaki and Liu 2016). However, overestimation of damage is observed in Kumamoto city.

In order to evaluate the performance of the method, Figure 6 shows the proposed threshold overlapped with the parameters (r and d) calculated for damaged and undamaged buildings estimated from Lidar data (Moya et al. 2016). Figure 6a shows the scatter plot of damaged (blue marks) and undamaged (red marks) buildings, where a complete overlap between them. This is the main reason of an overestimation in our results. The damaged and undamaged buildings are shown separate in Figure 6b and Figure 6c, respectively. The color shade express density of points, where the red color shows area whit high density. It is shown that our method is doing the best to separate the two areas in which the damaged and undamaged buildings are concentrating.

4. CONCLUSION

This paper presents a novel method that combines SAR imagery and strong motion distribution to estimate building damage. The fundamental basis of the method is that the final damage scenario estimated from a threshold of the parameters d and r should produce a logarithmic cumulative distribution function between the strong motion magnitude and the damage ratio.

Verification of the method during the 2016 Kumamoto earthquake has shown that the estimated threshold divided the main part of the undamaged buildings with the damaged buildings. However, the results show an overestimation of the damage distribution because the data set shows a remarkable overlapping between damaged and undamaged building.

It is important to point out the versatility of the method in the sense that it does not require training data

(unsupervised classification) and it can be used for other natural disaster as long as the EDP can be quantified. For instance, wave height can represent the EDP for a tsunami event.

References

- Adriano, B., Mas, E. and Koshimura, S., 2015. Developing a building damage function using SAR images and post-event data after the Typhoon Haiyan in The Philippines. *Journal of Japan Society of Civil Engineers, Ser. B2 (Coastal Engineering)*, 71(2), p.I 1729-I 1734.
- Koshimura, S., Oie, T., Yanagisawa, H., and Imamura, F., 2009. Developing Fragility Functions for Tsunami Damage Estimation Using Numerical Model and Post-Tsunami Data From Banda Aceh, Indonesia. *Coastal Engineering Journal*, 51(3), pp.243–273.
- Liu, W., Yamazaki, F., Gokon, H., and Koshimura, S., 2013. Extraction of tsunami-flooded areas and damaged buildings in the 2011 Tohoku-oki earthquake from TerraSAR-X intensity images. *Earthquake Spectra*, 29 (SUPPL.1), pp.183–200.
- Mas, E., Kosimura, S., Suppasri, A., Matsuoka, M., Matsuyama, M., Yoshii, T., Jimenez, C., Yamazaki, F., and Imamura, F., 2012. Developing Tsunami fragility curves using remote sensing and survey data of the 2010 Chilean Tsunami in Dichato. *Natural Hazards and Earth System Science*, 12(8), pp.2689–2697.
- Matsuoka, M. and Yamamoto, N., 2012. Web-based Quick Estimation System of Strong Ground Motion Maps Using Engineering Geomorphologic Classification Map and Observed Seismic Records. *15th World Conference on Earthquake Engineering*.
- Moya, L., Yamazaki, F., Liu, W., Tatsuro, C., and Mas, E., 2016. Detection of collapsed buildings due to the 2016 Kumamoto earthquake from Lidar data. *World Engineering Conference on Disaster reduction*, Lima, Peru, 8 pages.
- Yamazaki, F. and Liu, W., 2016. Remote sensing technologies for post-earthquake damage assessment: A case study on the 2016 Kumamoto earthquake. *6th ASIA Conference on Earthquake Engineering (6ACEE)*, pp.22–24.
- Yamazaki, F., and Murao, O., 2000. *Vulnerability functions for Japanese buildings based on damage data from the 1995 Kobe earthquake*, in Implications of recent earthquakes on seismic risk, pp. 91-101. Imperial College Press, London.

Acknowledgements

This research is supported by the Japan Science and Technology Agency (JST) through the SICORP project “Increasing Urban Resilience to Large Scale Disaster: The Development of a Dynamic Integrated Model for Disaster Management and Socio-Economic Analysis (DIM2SEA)” and the support of the International Research Institute of Disaster Science (IRIDeS) at Tohoku University.